



UNIVERSITY OF LEEDS

This is a repository copy of *High-power density, single plasmon, terahertz quantum cascade lasers via transverse mode control*.

White Rose Research Online URL for this paper:

<https://eprints.whiterose.ac.uk/198301/>

Version: Accepted Version

---

**Article:**

Song, C, Salih, M [orcid.org/0009-0001-6882-4642](https://orcid.org/0009-0001-6882-4642), Li, LH [orcid.org/0000-0003-4998-7259](https://orcid.org/0000-0003-4998-7259) et al. (5 more authors) (Cover date: 20 March 2023) High-power density, single plasmon, terahertz quantum cascade lasers via transverse mode control. *Applied Physics Letters*, 122 (12). 121108. ISSN 0003-6951

<https://doi.org/10.1063/5.0142359>

---

© 2023 Author(s). This article may be downloaded for personal use only. Any other use requires prior permission of the author and AIP Publishing. The following article appeared in C. Song, M. Salih, L. H. Li, J. Mangeney, J. Tignon, A. G. Davies, E. H. Linfield, S. Dhillon; High-power density, single plasmon, terahertz quantum cascade lasers via transverse mode control. *Appl. Phys. Lett.* 20 March 2023; 122 (12): 121108 and may be found at <https://doi.org/10.1063/5.0142359>. Uploaded in accordance with the publisher's self-archiving policy.

**Reuse**

Items deposited in White Rose Research Online are protected by copyright, with all rights reserved unless indicated otherwise. They may be downloaded and/or printed for private study, or other acts as permitted by national copyright laws. The publisher or other rights holders may allow further reproduction and re-use of the full text version. This is indicated by the licence information on the White Rose Research Online record for the item.

**Takedown**

If you consider content in White Rose Research Online to be in breach of UK law, please notify us by emailing [eprints@whiterose.ac.uk](mailto:eprints@whiterose.ac.uk) including the URL of the record and the reason for the withdrawal request.



[eprints@whiterose.ac.uk](mailto:eprints@whiterose.ac.uk)  
<https://eprints.whiterose.ac.uk/>

# High-power density, single plasmon, terahertz quantum cascade lasers via transverse mode control

C. Song<sup>1,#</sup>, M. Salih<sup>2,#</sup>, L. H. Li<sup>2</sup>, J. Mangeney<sup>1</sup>, J. Tignon<sup>1</sup>, A. G. Davies<sup>2</sup>, E. H. Linfield<sup>2</sup> and S. Dhillon<sup>1,\*</sup>

<sup>1</sup> Laboratoire de Physique de l'Ecole normale supérieure, ENS, Université PSL, CNRS, Sorbonne Université, Université de Paris, 24 rue Lhomond, 75005 Paris, France

<sup>2</sup> School of Electronic and Electrical Engineering, University of Leeds, Leeds LS2 9JT, United Kingdom

#: these authors contributed equally to work

\*Correspondance e-mail: sukhdeep.dhillon@ens.fr

**Abstract:** Terahertz (THz) quantum cascade lasers (QCLs) have been shown to emit peak powers greater than 1 W from a single facet in a single plasmon geometry. However, this is typically achieved by increasing the laser ridge width, resulting in higher-order transverse modes, limiting the achievable power density. Here we control and fully suppress these modes through thin metallic side-absorbers, showing laser action solely on the fundamental transverse mode operation without sacrificing high THz peak powers. This leads to enhanced power densities and electric fields of up to 1.8 kW/cm<sup>2</sup> and 1.17 kV/cm, respectively, opening up the possibility of applying THz QCLs as pump sources for investigations of non-linear THz physical phenomena.

The generation of intense terahertz (THz) frequency radiation has become an important domain to study THz nonlinear interactions in a variety of low energy phenomena ranging from high harmonic generation in Dirac materials<sup>1,2</sup> to spin excitations<sup>3,4</sup>. However, the THz sources used are based on down-conversion of extremely powerful, large and complex optical ultrafast lasers to the THz range<sup>5</sup> with little control of the central frequency and spectral bandwidth. THz quantum cascade lasers (QCLs), on the other hand, provide an electrically-driven, compact semiconductor source where the emission characteristics can be entirely chosen by design.

THz QCLs<sup>6</sup> are unipolar semiconductor lasers based on electronic intersubband transitions in multi-layered heterostructures. QCLs have shown considerable developments over recent years, from high temperature operation<sup>7-10</sup>, broad coverage of the THz range<sup>11,12</sup> to frequency comb operation<sup>13-16</sup>. Furthermore, in THz range, peak output powers of  $> 1\text{W}$  have been demonstrated from single plasmon waveguides<sup>17,18</sup>. Wafer bonded ridges have also shown 470mW output powers<sup>19</sup>. This was achieved using high performance thick (24  $\mu\text{m}$ ) active regions combined with large ridge widths ( $> 400\mu\text{m}$ ). However, large ridge widths will result in higher order transverse modes that can have negative side-effects for the laser. For example, different modes have different effective refractive indices, resulting in different group velocities and affecting the generation of ultra-short pulses<sup>20</sup>. Importantly for this work, higher order transverse modes will result in an uneven power distribution over the cavity and an multi-mode far-field<sup>20</sup>. This will in turn result a large spot size when focused and hence a reduced power density when compared to the fundamental mode. These higher order modes then are detrimental for the observation of THz nonlinear phenomena.

Previous work on transverse mode control has been applied to metal-metal THz QCLs using doped or thin metallic (a few nanometers) ridge side-absorbers that are placed on the extremity of the ridge and along the entirety of the laser cavity<sup>20,21</sup>. These permit to increase the THz losses on higher order modes without effecting the fundamental mode, resulting in laser action only on the latter. However, as this approach has only been applied to metal-metal waveguides, the resulting output power densities remain relatively low. Other methods to control the modal profile include structuring of the top metal of metal-metal waveguides<sup>22</sup> or metasurfaces<sup>23</sup> for high power surface emission. Here, we demonstrate single transverse mode operation from single plasmon THz QCLs with  $>1\text{W}$  peak output powers using thin nickel side-absorbers. This permits to increase the losses on higher order modes with little effect on the emitted peak powers and therefore enhancing the power density. Although THz nonlinear interactions have been investigated using THz QCLs through up-conversion and down-conversion<sup>24-26</sup>, this has been based on the inherent QCL nonlinearities within a QCL cavity where the power density is high. The work here opens interesting perspectives

for investigating THz nonlinearities using these compact laser systems as external pump sources.

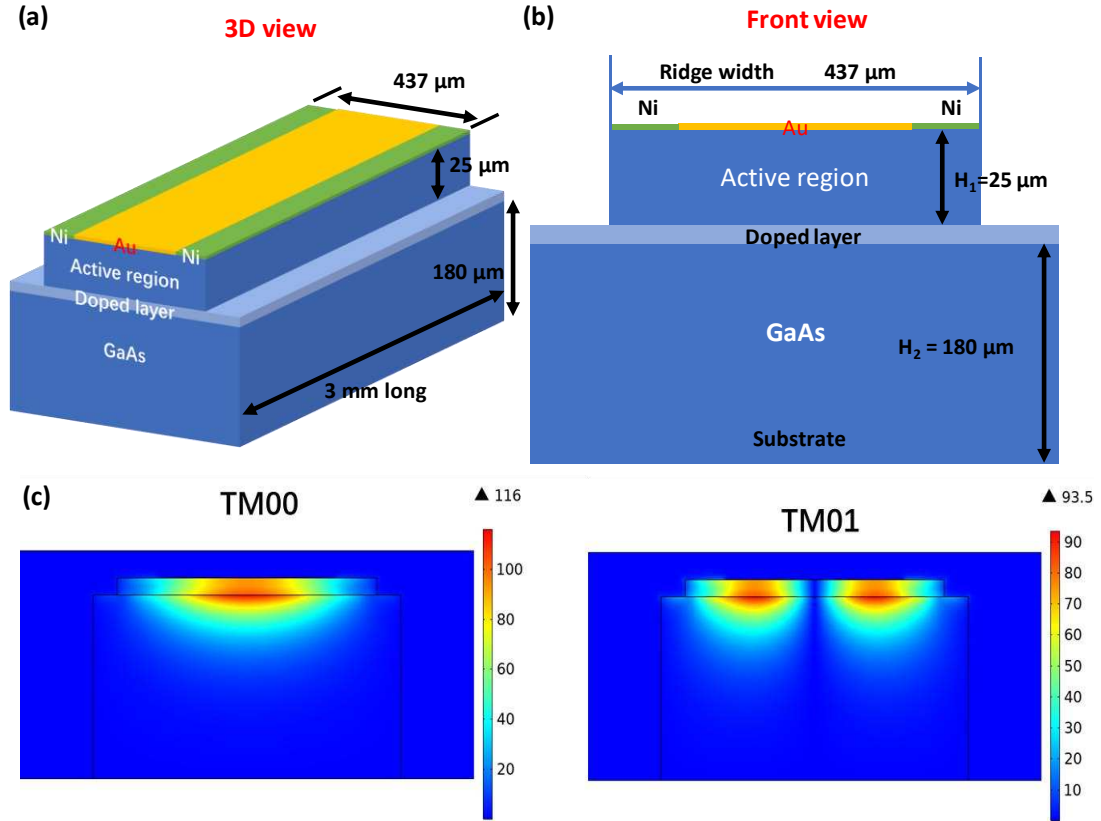


**Figure 1.** Schematic of the single plasmon THz QCLs with a (a) 3D view and (b) Front view with Ni side-absorbers to limit higher order modes. (Top doped layer not shown). (c) Calculated mode profiles of fundamental mode  $TM_{00}$  and first high order mode  $TM_{01}$ .

Two dimensional electromagnetic simulations (COMSOL Multiphysics) were used to illustrate the impact of lossy side-absorbers on THz QCLs structures and to determine the threshold gain. The geometry investigated is shown in figure 1(a) and (b). The ridge thickness and width here was  $25\mu\text{m}$  and  $440\mu\text{m}$ , respectively. A 5 nm thick nickel side-absorber was introduced along the entire length of the two edges of the ridge with various widths in order to increase the difference in losses between the fundamental and higher order transverse modes, permitting to suppress laser action on the higher-order competing modes. The Ni layer was modelled using its complex refractive indices. (Other thin lossy metals such as Pt could also be used). The upper gold contact layer

was 150 nm thick. The lower 700 nm heavily Si-doped ( $2 \times 10^{18} \text{ cm}^{-3}$ ) GaAs contact layer lies between the active region and substrate (thickness  $\sim 180 \mu\text{m}$ ). The upper doped layer is Si-doped to  $5 \times 10^{18} \text{ cm}^{-3}$  and a thickness of 70 nm. Frequency-dependent simulations were performed in order to adapt them to broadband emission of THz QCLs. Figure 1(c) shows the simulated fundamental and higher order modes (TM<sub>00</sub> and TM<sub>01</sub>).

The threshold gain  $g_{th}$  is defined as <sup>27</sup>:

$$g_{th} = \frac{\alpha_m(\nu) + \alpha_w(\nu)}{\Gamma(\nu)} \quad (1)$$

where  $\alpha_m$  presents the mirror losses and  $\alpha_w$  indicates the waveguide losses of the laser cavity.  $\Gamma$  represents the confinement factor of the electric field with the active region. The mirror losses  $\alpha_m$  can be expressed as:

$$\alpha_m(\nu) = -\ln(R_1 R_2)/2L \quad (2)$$

where  $R_1$  and  $R_2$  are the front and back facet reflectivity,  $L$  is the cavity length. The waveguide losses  $\alpha_w$  can be expressed as:

$$\alpha_w(\nu) = \frac{4\pi}{\lambda} k(\nu) \quad (3)$$

where  $k$  represents extinction coefficient of the modes propagating in the waveguide. The confinement factor  $\Gamma$  can be defined as the ratio of the overlap of the mode with the active region to that over the total intensity <sup>20</sup>:

$$\Gamma(\nu) = \frac{\int dy dx E_y^2(y, x, \nu) \varepsilon(y, x, \nu)}{\int_{y,x=-\infty}^{\infty} dy dx E^2(y, x, \nu) \varepsilon(y, x, \nu)} \quad (4)$$

where  $E(y, x, \nu)$  is the electric field at position  $(y, x)$  with a frequency  $\nu$ ,  $E_y(y, x, \nu)$  is the part of the electric field that couples to the intersubband transition, and  $\varepsilon(y, x, \nu)$  is the dielectric function at the frequency  $\nu$ .

Here the width of nickel side-absorbers was varied as  $0 \mu\text{m}$  (reference),  $20 \mu\text{m}$ ,  $40 \mu\text{m}$  to  $60 \mu\text{m}$ . Figure 2(a) shows that the confinement factor as a function of frequency

with only small decrease of about 0.04 with the nickel width increasing from 0 to 60  $\mu\text{m}$  (ridge width 420  $\mu\text{m}$ ), indicating that the side-absorbers have little influence on the overlap factor. Figure 2(b) shows the much stronger impact of the different side-absorbers on the waveguide losses. When there is no nickel side-absorbers, the difference of waveguide losses between  $\text{TM}_{00}$  and  $\text{TM}_{01}$  is small. However, as the width of lossy side-absorbers increases to 20  $\mu\text{m}$ , 40  $\mu\text{m}$  and 60  $\mu\text{m}$ , the difference between the losses of  $\text{TM}_{00}$  and  $\text{TM}_{01}$  mode increases. For example, the waveguide loss of  $\text{TM}_{01}$  ( $> 8 \text{ cm}^{-1}$ ) is more than twice that of  $\text{TM}_{00}$  ( $\sim 4 \text{ cm}^{-1}$ ) with 60 $\mu\text{m}$  wide side-absorbers. This will mean that the higher order  $\text{TM}_{01}$  mode will be suppressed, favoring laser action on the fundamental mode only. Higher order modes ( $> \text{TM}_{01}$ ) have higher losses and will therefore be suppressed. (Since the QCLs discussed here have the same long cavity length and processed from the same material, the mirror losses are low and similar between the modes<sup>28,29</sup>).

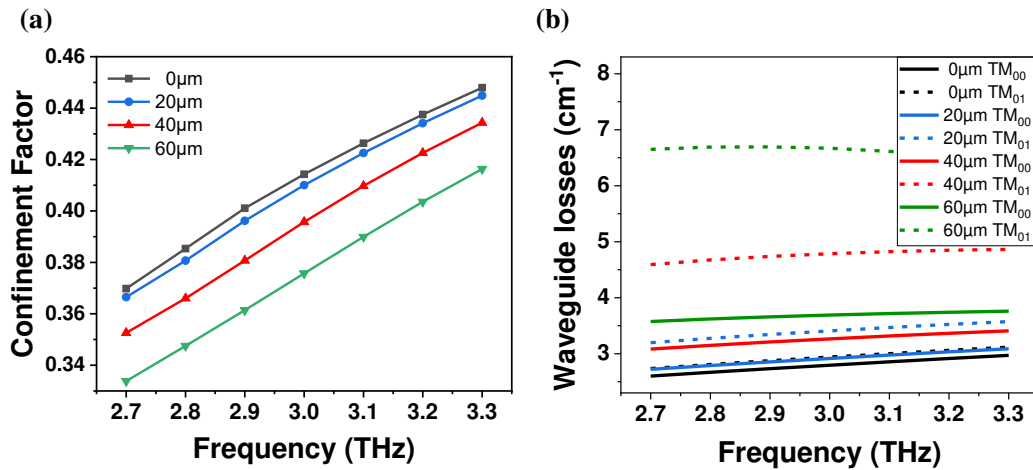


**Figure 2.** (a) Confinement factor and (b) waveguide losses of the QCL with different side-absorbers widths. Solid lines are calculations for  $\text{TM}_{00}$  modes and dashed lines are for  $\text{TM}_{01}$  modes.

The THz QCL investigated is based on a hybrid active region (Bound-To-Continuum - Resonant-Phonon)<sup>30</sup> operating at  $\sim 3.2$  THz, with a 25  $\mu\text{m}$  thick active region ( $\sim 190$  periods). The THz QCLs were processed into the surface-plasmon ridge waveguide structures using photolithography and wet chemical etching. A 5 nm thick nickel side-absorber was introduced along the entire length of the two edges of the ridge with various widths (20  $\mu\text{m}$ , 40  $\mu\text{m}$  and 60  $\mu\text{m}$ ). There was an overlap of 3  $\mu\text{m}$  between

the nickel side-absorber, and the upper gold contact layer, which was 150 nm thick. Two set of ridges with widths of 399  $\mu\text{m}$  and 437  $\mu\text{m}$  were formed. The 700 nm heavily Si-doped ( $2 \times 10^{18} \text{ cm}^{-3}$ ) GaAs contact layer was contacted with annealed AuGeNi side contacts. The substrate was thinned to  $\sim 180 \mu\text{m}$  by wet chemical etching to improve heat dissipation. The devices were also cleaved into 3mm long cavities, wire bonded and indium-soldered to copper submounts for measurement (figure 3(a)). Figure 3(b), is the optical microscope images of THz QCLs (437  $\mu\text{m}$  ridge width) with and without side-absorbers, where the nickel side-absorbers are visible in the former.

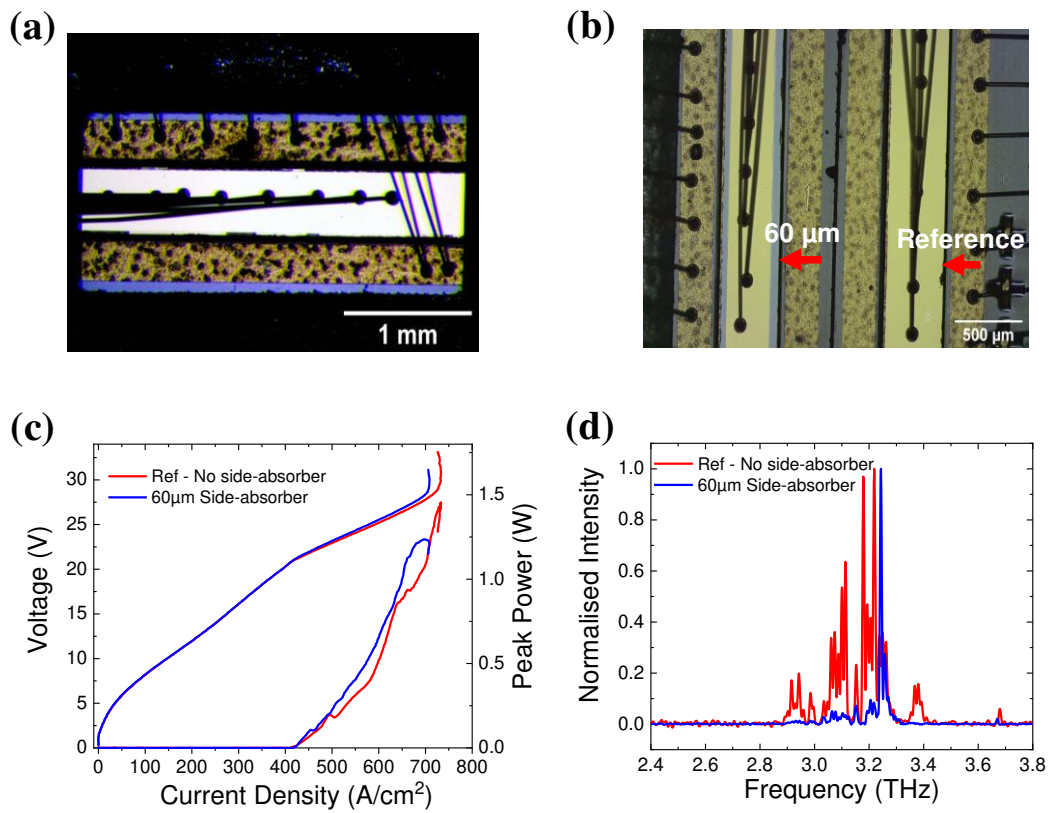


**Figure 3.** The optical microscope images of (a) the entire reference QCL (without side-absorbers), and (b) zoom showing QCLs with 60  $\mu\text{m}$  (left) wide side-absorbers and the reference (right) (437  $\mu\text{m}$  ridge width). (c) Voltage-current/current density and peak power-current/current density characteristics of THz QCLs without (red) and with 60  $\mu\text{m}$  (blue) side-absorbers. (d) Spectrum of QCLs without (red at 709  $\text{A}/\text{cm}^2$ ) and with 60  $\mu\text{m}$  (blue at 671  $\text{A}/\text{cm}^2$ ) side-absorbers for a 437  $\mu\text{m}$  ridge width.

The THz QCLs were characterized in pulsed mode, with a repetition rate of 10 kHz and a duty cycle of 2%, electrically gated by a 167 Hz square-wave for THz detection, in a liquid-helium continuous-flow cryostat (temperature  $\sim 10\text{K}$ ) equipped with 3 mm-

thick poly-4-methylpentene (TPX) windows. The radiation was collected and focused from a single facet with two plastic Zeonex lenses ( $f=50$  mm). The power was measured using an absolute THz power meter (Thomas Keating Ltd.) directly in front of the cryostat window. Figure 3(c) shows the voltage-current/current density and peak power–current/current density characteristics of THz QCL reference and with 60  $\mu\text{m}$  side-absorbers (ridge width 437  $\mu\text{m}$ ). Similar results were found for the other side absorbers. The peak power for the device without side-absorber was 1.45 W, with a small reduction (to 1.23 W) observed when the side-absorbers were incorporated. Figure 3(d) shows the frequency spectrum of the QCLs, showing a central frequency of emission of 3.2 THz. The side-absorber shows a smaller spectral bandwidth, possibly a result of the suppression of the higher order modes (see below). A similar spectrum is obtained for the thinner ridge.

To categorically show that higher modes are suppressed leading to higher power densities, we investigated the THz focused beam pattern of the realized QCLs. The focused beam was characterized using a THz camera (SwissTHz, model S2X) and two 50 mm focusing length lenses placed between the cryostat and THz camera. As can be observed from Figure 4(a) for the 437  $\mu\text{m}$  ridge width, the reference sample (no side-absorbers) show two focused spots, corresponding to laser action on a higher order mode. However, as the width of the side-absorbers is increased to 60  $\mu\text{m}$ , a single focused spot can be realized. The cut profiles in the ‘x’ direction (parallel to the QCL ridge surface) at the peak amplitude of the QCL intensity with the different side-absorber width are shown in Fig 4(c). Here it is shown that the beam spot width decreases with increasing width of side-absorbers from 0  $\mu\text{m}$ , 20  $\mu\text{m}$ , 40  $\mu\text{m}$  to 60  $\mu\text{m}$ , with a single lobe appearing for the widest side-absorber. (The full width at half maximum in the ‘y’ direction was 350  $\mu\text{m}$ , 350  $\mu\text{m}$ , 325  $\mu\text{m}$  and 250  $\mu\text{m}$ , respectively). A similar behavior was observed for the THz QCLs with 399  $\mu\text{m}$  ridge width. The experimental results clearly show that the higher order modes are suppressed via the addition of nickel side-absorbers.

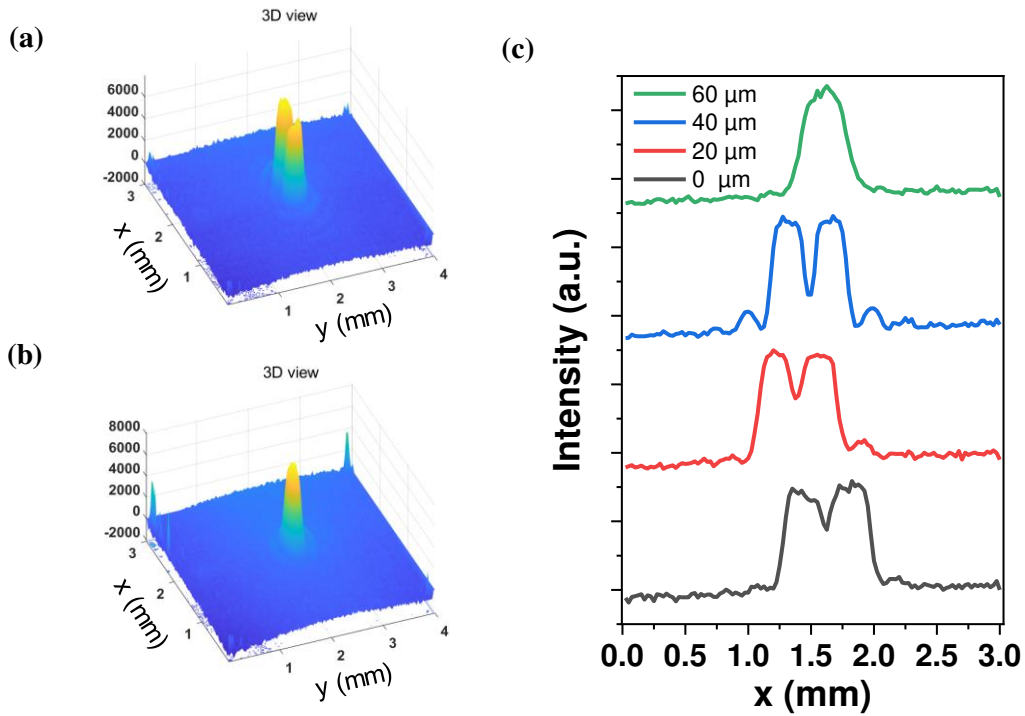


Figure 4. Focused beam 3D view profiles from 437  $\mu\text{m}$  wide QCLs (a) without and (b) with 60  $\mu\text{m}$  nickel side-absorber (c) Cut profile in 'x' (parallel to QCL ridge surface) at the peak intensity of the QCL beam with the different side-absorber widths (offset for clarity).

From the acquired spot profiles and the measured peak powers, the THz power densities can be obtained. The spot profiles were fitted with a Gaussian curve (single Gaussian for the 60  $\mu\text{m}$  side absorber QCL, double Gaussian for the other samples) to determine the spot area. This was performed for the two sets of ridges (399  $\mu\text{m}$  and 437  $\mu\text{m}$  ridge). Figure 5 summarizes all samples and shows that the power density increases from 0.63  $\text{kW}/\text{cm}^2$  to 1.07  $\text{kW}/\text{cm}^2$  as the nickel side-absorber width is increased from 0  $\mu\text{m}$  to 60  $\mu\text{m}$  for ridges of 399  $\mu\text{m}$  width. For the QCL ridges of 437  $\mu\text{m}$  width, the power density increases from 0.995  $\text{kW}/\text{cm}^2$  to 1.8  $\text{kW}/\text{cm}^2$  illustrating that the power density is can be significantly enhanced with the correct nickel side-absorbers. The corresponding electric field of the highest power is determined to be 1.17  $\text{kV}/\text{cm}$  (from  $P = E^2/(2Z_0)$  where  $P$  is the power density,  $E$  the peak electric field and  $Z_0$  is the impedance of free space (377  $\Omega$ )). (Further increases in

side-absorber width is not expected to increase the power density owing to increased losses and reduced overlap). For comparison, although THz pulsed systems based on amplified femtosecond pulses can reach higher peak power densities, this is over a broad spectral distribution and centered typically around 1 THz.

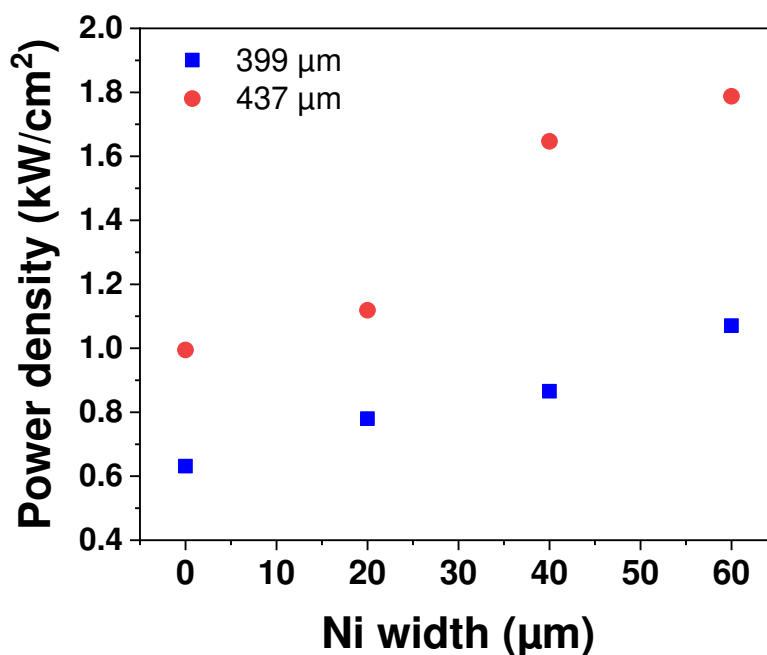


Fig 5. QCL Power density as a function of nickel side-absorber width for 399  $\mu\text{m}$  (blue) and 437  $\mu\text{m}$  (red) wide ridges. All devices were 3mm long.

In this work we have shown that high power densities can be realized from single plasmon THz QCLs, limiting the effect of high order modes despite the use of very wide laser ridges. This was achieved using lossy nickel side-absorbers that increase the losses of higher order transverse modes without effecting the fundamental mode. A THz camera was used to show control of the THz spot form and dimensions. The application of these side-absorbers permits the power density to be almost doubled when compared to the case without side-absorbers, reaching  $1.8 \text{ kW/cm}^2$ , corresponding to electric fields  $\sim 1.17 \text{ kV/cm}$ . Further enhancements can be achieved through HR coatings on the back facet, wider ridges, smaller  $f\#$  optics, as well as combining the THz QCL emission with metasurfaces or resonators. The latter approach has shown that THz electric fields can be enhanced by more than an order of magnitude<sup>31,32</sup>. This could

be used to realise fields exceeding tens of kV/cm that compares favourably with recent work using FEL to study harmonic generation in graphene, which required a field of  $\sim 10$  kV/cm for observation of the third harmonic<sup>1</sup>. This resonator approach could also be combined with THz pulse generation through QCL modelocking for further enhancements of the peak power densities and ultrafast excitations<sup>33,34</sup>. This work therefore will be particularly important in the application of THz QCLs as a compact pump source for the study of non-linear THz physical phenomena where high power densities are vital.

The authors acknowledge funding from European Union's Horizon 2020 research and innovation program under grant agreement No 964735 (FET-OPEN EXTREME-IR), and the French National Research Agency (ANR-18-CE24-0013-02 - "TERASEL"). C. Song acknowledges support from the China Scholarship Council (Grant No. 201804910824).

<sup>1</sup> H.A. Hafez, S. Kovalev, J.-C. Deinert, Z. Mics, B. Green, N. Awari, M. Chen, S. Germanskiy, U. Lehnert, J. Teichert, Z. Wang, K.-J. Tielrooij, Z. Liu, Z. Chen, A. Narita, K. Müllen, M. Bonn, M. Gensch, and D. Turchinovich, *Nature* **561**, 507 (2018).

<sup>2</sup> B. Cheng, N. Kanda, T.N. Ikeda, T. Matsuda, P. Xia, T. Schumann, S. Stemmer, J. Itatani, N.P. Armitage, and R. Matsunaga, *Phys. Rev. Lett.* **124**, 117402 (2020).

<sup>3</sup> T. Kampfrath, A. Sell, G. Klatt, A. Pashkin, S. Mahrlein, T. Dekorsy, M. Wolf, M. Fiebig, A. Leitenstorfer, and R. Huber, *Nat Photon* **5**, 31 (2011).

<sup>4</sup> T. Kampfrath, K. Tanaka, and K.A. Nelson, *Nature Photonics* **7**, 680 (2013).

<sup>5</sup> H.A. Hafez, X. Chai, A. Ibrahim, S. Mondal, D. Férachou, X. Ropagnol, and T. Ozaki, *J. Opt.* **18**, 093004 (2016).

<sup>6</sup> R. Köhler, A. Tredicucci, F. Beltram, H.E. Beere, E.H. Linfield, A.G. Davies, D.A. Ritchie, R.C. Iotti, and F. Rossi, *Nature* **417**, 156 (2002).

<sup>7</sup> B. Wen and D. Ban, *Progress in Quantum Electronics* **80**, 100363 (2021).

<sup>8</sup> A. Khalatpour, A.K. Paulsen, C. Deimert, Z.R. Wasilewski, and Q. Hu, *Nature Photonics* (2020).

<sup>9</sup> M.A. Kainz, M.P. Semtsiv, G. Tsianos, S. Kurllov, W.T. Masselink, S. Schönhuber, H. Detz, W. Schrenk, K. Unterrainer, G. Strasser, and A.M. Andrews, *Opt. Express* **27**, 20688 (2019).

<sup>10</sup> L. Bosco, M. Franckić, G. Scalari, M. Beck, A. Wacker, and J. Faist, *Appl. Phys. Lett.* **115**, 010601 (2019).

<sup>11</sup> S.S. Dhillon, M.S. Vitiello, E.H. Linfield, A.G. Davies, M.C. Hoffmann, J. Booske,

C. Paoloni, M. Gensch, P. Weightman, G.P. Williams, E. Castro-Camus, D.R.S. Cumming, F. Simoens, I. Escorcia-Carranza, J. Grant, S. Lucyszyn, M. Kuwata-Gonokami, K. Konishi, M. Koch, C.A. Schmuttenmaer, T.L. Cocker, R. Huber, A.G. Markelz, Z.D. Taylor, V.P. Wallace, J. Axel Zeitler, J. Sibik, T.M. Korter, B. Ellison, S. Rea, P. Goldsmith, K.B. Cooper, R. Appleby, D. Pardo, P.G. Huggard, V. Krozer, H. Shams, M. Fice, C. Renaud, A. Seeds, A. Stöhr, M. Naftaly, N. Ridler, R. Clarke, J.E. Cunningham, and M.B. Johnston, *J. Phys. D: Appl. Phys.* **50**, 043001 (2017).

<sup>12</sup> C.A. Curwen, J.L. Reno, and B.S. Williams, *Nature Photonics* **13**, 855 (2019).

<sup>13</sup> D. Burghoff, T.-Y. Kao, N. Han, C.W.I. Chan, X. Cai, Y. Yang, D.J. Hayton, J.-R. Gao, J.L. Reno, and Q. Hu, *Nature Photon* **8**, 462 (2014).

<sup>14</sup> M. Rösch, G. Scalari, M. Beck, and J. Faist, *Nat Photon* **9**, 42 (2015).

<sup>15</sup> L. Consolino, M. Nafa, F. Cappelli, K. Garrasi, F.P. Mezzapesa, L. Li, A.G. Davies, E.H. Linfield, M.S. Vitiello, P. De Natale, and S. Bartalini, *Nat Commun* **10**, 2938 (2019).

<sup>16</sup> F.P. Mezzapesa, V. Pistore, K. Garrasi, L. Li, A.G. Davies, E.H. Linfield, S. Dhillon, and M.S. Vitiello, *Opt. Express* **27**, 20231 (2019).

<sup>17</sup> L. h. Li, L. Chen, J. r. Freeman, M. Salih, P. Dean, A. g. Davies, and E. h. Linfield, *Electronics Letters* **53**, 799 (2017).

<sup>18</sup> L. Li, L. Chen, J. Zhu, J. Freeman, P. Dean, A. Valavanis, A. g. Davies, and E. h. Linfield, *Electronics Letters* **50**, 309 (2014).

<sup>19</sup> M. Brandstetter, C. Deutsch, M. Krall, H. Detz, D.C. MacFarland, T. Zederbauer, A.M. Andrews, W. Schrenk, G. Strasser, and K. Unterrainer, *Appl. Phys. Lett.* **103**, 171113 (2013).

<sup>20</sup> D. Bachmann, M. Rösch, M.J. Süess, M. Beck, K. Unterrainer, J. Darmo, J. Faist, and G. Scalari, *Optica* **3**, 1087 (2016).

<sup>21</sup> J.A. Fan, M.A. Belkin, F. Capasso, S.P. Khanna, M. Lachab, A.G. Davies, and E.H. Linfield, *Appl. Phys. Lett.* **92**, 031106 (2008).

<sup>22</sup> M.S. Vitiello and A. Tredicucci, *Advances in Physics: X* **6**, 1893809 (2021).

<sup>23</sup> C.A. Curwen, J.L. Reno, and B.S. Williams, *Appl. Phys. Lett.* **113**, 011104 (2018).

<sup>24</sup> V. Pistore, H. Nong, P.-B. Vigneron, K. Garrasi, S. Houver, L. Li, A. Giles Davies, E.H. Linfield, J. Tignon, J. Mangeney, R. Colombelli, M.S. Vitiello, and S.S. Dhillon, *Nature Communications* **12**, 1427 (2021).

<sup>25</sup> J. Madéo, P. Cavalie, J.R. Freeman, N. Jukam, J. Maysonnave, K. Maussang, Harvey.E. Beere, D.A. Ritchie, C. Sirtori, J. Tignon, and S.S. Dhillon, *Nature Photonics* **6**, 519 (2012).

<sup>26</sup> S. Houver, A. Lebreton, T.A.S. Pereira, G. Xu, R. Colombelli, I. Kundu, L.H. Li, E.H. Linfield, A.G. Davies, J. Mangeney, J. Tignon, R. Ferreira, and S.S. Dhillon, *Sci Adv* **5**, eaaw7554 (2019).

<sup>27</sup> J. Faist, *Quantum Cascade Lasers* (Quantum Cascade Lasers, 2013).

<sup>28</sup> S. Fatholouloumi, E. Dupont, S.G. Razavipour, S.R. Laframboise, A. Delage, Z.R. Wasilewski, A. Bezinger, G.Z. Rafi, S. Safavi-Naeini, D. Ban, and H.C. Liu, *Opt. Express* **18**, 10036 (2010).

<sup>29</sup> S. Kohen, B.S. Williams, and Q. Hu, *Journal of Applied Physics* **97**, 053106 (2005).

<sup>30</sup> M.I. Amanti, G. Scalari, R. Terazzi, M. Fischer, M. Beck, J. Faist, A. Rudra, P. Gallo,

and E. Kapon, *New J. Phys.* **11**, 125022 (2009).

<sup>31</sup> I. Al-Naib and W. Withayachumnankul, *Journal of Infrared, Millimeter, and Terahertz Waves* **38**, 1067 (2017).

<sup>32</sup> Y.-M. Bahk, D.J. Park, and D.-S. Kim, *Journal of Applied Physics* **126**, 120901 (2019).

<sup>33</sup> F. Wang, H. Nong, T. Fobbe, V. Pistore, S. Houver, S. Markmann, N. Jukam, M. Amanti, C. Sirtori, S. Moumdji, R. Colombelli, L. Li, E. Linfield, G. Davies, J. Mangeney, J. Tignon, and S. Dhillon, *Laser & Photonics Reviews* **11**, 1700013 (2017).

<sup>34</sup> J.R. Freeman, J. Maysonave, H.E. Beere, D.A. Ritchie, J. Tignon, and S.S. Dhillon, *Optics Express* **21**, 16162 (2013).